Water Research 294 (2026) 125562

Contents lists available at ScienceDirect

Water Research

journal homepage: www.elsevier.com/locate/watres

Long-term observations uncover sustained carbon dioxide emissions from lakes following aquaculture retreat

Jiayu Zhao [a,b,c], Mi Zhang [d], Wei Xiao [c,d], Pei Ge [d], Juhua Luo [e], Minliang Jiang [e], Cheng Hu [f], Delin Li [a,b], Tianyu Zhang [a], Hongtao Duan [e], Qitao Xiao [e,*], Xuhui Lee [g]

[a] College of Ocean and Meteorology, Guangdong Ocean University, Zhanjiang 524088, China
[b] South China Sea Institute of Marine Meteorology (SIMM), Guangdong Ocean University, Zhanjiang 524088, China
[c] Collaborative Innovation Center on Forecast and Evaluation of Meteorological Disasters (CIC-FEMD), Nanjing University of Information Science & Technology, Nanjing 210044, China
[d] Yale-NUIST Center on Atmospheric Environment, Nanjing University of Information Science & Technology, Nanjing 210044, China
[e] State Key Laboratory of Lake and Watershed Science for Water Security, Nanjing Institute of Geography and Limnology, Chinese Academy of Sciences, Nanjing 211135, China
[f] College of Ecology and the Environment, Joint Center for sustainable Forestry in Southern China, Nanjing Forestry University, Nanjing 210037, China
[g] School of the Environment, Yale University, New Haven 06511, USA

HIGHLIGHTS

- CO_2 variability of aquaculture-affected lakes was investigated at a decadal scale.
- Aquaculture-affected lakes acted as significant CO_2 sources.
- Nutrient enrichment contributed to significant CO_2 emissions.
- Sustained CO_2 emissions persisted following aquaculture retreat.
- Random Forest model identified nutrient loading and aquaculture area as key predictors.

GRAPHICAL ABSTRACT

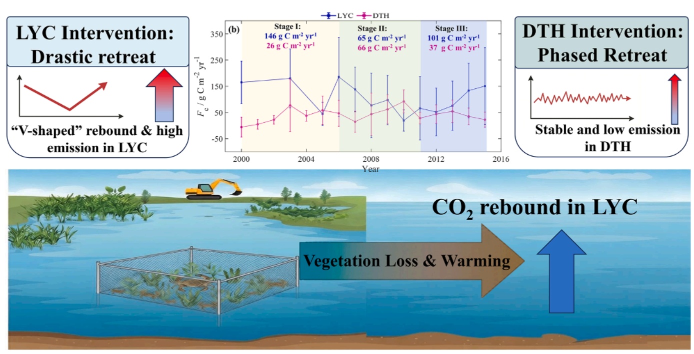

ARTICLE INFO

Keywords:
CO_2 dynamics
Lake aquaculture
Long-term measurements
Aquaculture retreat
Random forest model

ABSTRACT

Aquaculture has emerged as one of the dominant anthropogenic drivers altering the carbon dioxide (CO_2) balance of lake ecosystems. Although aquaculture retreat (pen removal) has been widely implemented in lakes, its long-term effects on CO_2 variability remain poorly constrained due to insufficient field measurements, thereby hindering our understanding of anthropogenic carbon cycling. To address this knowledge gap, we investigated the partial pressure of carbon dioxide (pCO_2) and CO_2 flux in two typical aquaculture-affected lakes in eastern China (Lake Yangcheng, LYC; Dongtaihu Bay of Lake Taihu, DTH) based on long-term (2000–2015) field measurements. Results revealed that both systems were net CO_2 sources, yet LYC with high nutrient loadings exhibited significantly higher emissions (108 ± 56 g C m^{-2} yr^{-1}; pCO_2: 1180 ± 390 μatm) than DTH (37 ± 24 g C m^{-2} yr^{-1}; pCO_2: 716 ± 185 μatm). Crucially, CO_2 emissions in LYC exhibited a counter-intuitive "V-shaped"

* Corresponding author.
E-mail address: qtxiao@niglas.ac.cn (Q. Xiao).

https://doi.org/10.1016/j.watres.2026.125562
Received 19 December 2025; Received in revised form 9 February 2026; Accepted 11 February 2026
Available online 12 February 2026

trajectory in response to management interventions: declining by 54 % during the active removal phase, but rebounding by 56 % in the post-restoration phase. This unexpected rebound was driven not merely by nutrient legacy, but fundamentally by the loss of submerged vegetation, thereby severely compromising the ecosystem's CO_2 uptake capacity. In contrast, DTH maintained stable emissions under a moderate retreat strategy mostly due to the stabilizing effect of macrophyte retention. The Random Forest (RF) model further showed that aquaculture area functions as a non-linear regulator of emission intensity, challenging linear scaling assumptions. Our findings demonstrate that successful carbon mitigation in aquaculture systems relies not merely on nutrient load reduction but fundamentally on the structural recovery and functional integrity of the autotrophic carbon sink.

1. Introduction

Lakes account for only 2.2 % of the Earth's land surface but play a pivotal role in the global carbon dioxide (CO_2) budget (Raymond et al., 2013; Holgerson and Raymond, 2016; Pi et al., 2022). Lakes are generally supersaturated with CO_2 and are widely recognized as sources of CO_2 emissions (Borges et al., 2022; Duan et al., 2023; Lauerwald et al., 2023). Over the past decade, substantial effort has been made to refine emission estimates at both regional and global scales (e.g., Finlay et al., 2015; Li et al., 2018; Song et al., 2024; Grasset et al., 2025; Zhang et al., 2026b). However, current CO_2 emission estimates for global lakes remain highly uncertain, spanning over one order of magnitude from 0.07 to 0.81 Pg C yr^{-1} (Cole et al., 2007; Raymond et al., 2013; DelSontro et al., 2018; Lauerwald et al., 2023). This large uncertainty arises not only from observational limitations but also from the profound yet poorly quantified influence of human activities, which alter lake biogeochemistry and consequently dramatically impact CO_2 emissions (Liu et al., 2025b; Zhang et al., 2026b). Considering that human activity can reshape lake CO_2 emissions, there is an urgent need for more comprehensive field-based measurements to quantify these anthropogenic impacts on CO_2 dynamics.

Pen aquaculture has become a dominant anthropogenic influence on lake ecosystems since the late 1980s, driven by rising global demand for aquatic protein (FAO, 2024). This intensive practice significantly alters lake carbon dynamics through complex and opposing biogeochemical pathways (Kosten et al., 2020; Chen et al., 2023; Zhang et al., 2026a). On one hand, the intentional introduction of submerged macrophytes for habitat enhancement promotes photosynthetic CO_2 uptake, with well-vegetated zones reducing emissions by up to 43 % compared to barren areas (Zhang et al., 2022b). On the other hand, substantial feed inputs (1500 to 6000 kg C ha^{-1} yr^{-1}) stimulate microbial respiration and thus enhance CO_2 efflux (Chen et al., 2016; Yuan et al., 2019; Waldemer and Koschorreck, 2023; Yang et al., 2024; Liu et al., 2025a). While existing research has extensively debated this "source-sink" balance during the active phase of aquaculture, a critical yet overlooked dimension is the ecological transition triggered by the cessation of these activities. The implementation of "aquaculture retreat" policies, which are designed to restore water quality, essentially acts as a massive environmental disturbance, leading to the dismantling of over 83 % of enclosures in subtropical lakes (Luo et al., 2020; Yin et al., 2024). While such interventions initially mitigate external nutrient loading, they also abruptly terminate long-standing human-managed carbon sinks (Pu et al., 2022). It remains poorly understood how this sudden shift from intensive interference to natural recovery disrupts the established biogeochemical balance, and whether the subsequent variations in nutrient and macrophyte dynamics trigger potential regime shifts or non-linear trajectories in CO_2 dynamics.

A critical challenge in quantifying the impact of human activities on lake CO_2 dynamics is the lack of long-term observational data, particularly for specific management interventions. While the decadal-scale ecological responses to restoration in general eutrophic lakes have been increasingly reported, these studies have predominantly focused on water quality improvements or vegetation recovery (e.g., Lin et al., 2021; Duan et al., 2022; Poikane et al., 2024), with comparatively limited attention paid to the temporal evolution of carbon dynamics (e.g., Xiao et al., 2020, 2023). This knowledge gap is particularly acute for restored aquaculture systems, where the biogeochemical consequences remain poorly constrained (Kosten et al., 2020; Chen et al., 2023; Zhang et al., 2026a). Furthermore, given that aquaculture zones differ fundamentally from typical lake ecosystems in ecological structure and function, characterized by semi-enclosed physical barriers and substantial allochthonous nutrient subsidies (Pu et al., 2022; Zhao et al., 2025), it remains uncertain whether the conclusions derived from general lake restoration are directly applicable to these unique systems. This uncertainty is critically compounded by the prevalence of short-term observations (< 2 years) in existing literature, which are prone to misinterpreting transient states as stable trends and failing to capture complex lag effects (e.g., hysteresis) as the system transitions toward a new equilibrium (Jeppesen et al., 2007; Kosten et al., 2020). Therefore, long-term datasets are imperative to distinguish between temporary fluctuations and genuine regime shifts following the retreat of intensive aquaculture.

As the world's leading producer of freshwater aquaculture, China accounts for over 60 % of global output (FAO, 2024). The Yangtze River Delta (YRD) is a key region in China, contributing 26 % of China's aquaculture area (China Fishery Statistical Yearbook, 2023). Within this region, Lake Yangcheng (LYC) and Dongtaihu Bay of Lake Taihu (DTH) represent two prominent systems with long histories of aquaculture. Pen farming was initiated in both lakes in the 1980s, followed by rapid expansion. However, their developmental trajectories diverged significantly after 2008: LYC was subjected to drastic aquaculture removal initiatives, whereas DTH underwent a slower, phased retreat process (Luo et al., 2020; Xiao et al., 2024b). This contrast enables a systematic examination of how varying intensities of anthropogenic intervention influence carbon fluxes. By comparing the rapid policy-driven restoration in LYC with the gradual reduction in DTH, this study elucidates how different management strategies regulate lake carbon budgets. These findings provide a mechanistic understanding of carbon source-sink transitions across varying ecological recovery pathways.

To address the aforementioned gaps, this study presents a 16-year (2000–2015) dataset of partial pressure of carbon dioxide (pCO_2) measurements and CO_2 exchange flux estimates at the LYC and DTH sites. While freshwater aquaculture expansion is known to increase CO_2 emissions (Liu et al., 2025a;Yuan et al., 2019, 2025; Zhang et al., 2026a), we hypothesize that aquaculture retreat would trigger a continuous decline in CO_2 emissions. Therefore, the specific objectives of this study are: (1) to quantify the long-term CO_2 exchange fluxes and assess the carbon source/sink status of LYC and DTH over a 16-year period, (2) to characterize the interannual trajectories of CO_2 dynamics and determine whether "aquaculture retreat" triggers linear declines or non-linear regime shifts in carbon emissions, and (3) to identify the key environmental drivers and biological mechanisms that regulate CO_2 variability and develop predictive models. By integrating long-term observations and mechanistic analysis, this work aims to advance our understanding of carbon cycling in managed aquatic ecosystems and elucidate the complex biogeochemical feedbacks following anthropogenic disturbances.

2. Materials and methods

2.1. Site description

Lake Yangcheng (LYC) and Dongtaihu Bay of Lake Taihu (DTH) are two representative shallow eutrophic lakes located in the Yangtze River Delta, China (Fig. 1). LYC (31°21′ N, 120°39′ E) is the third-largest waterbody in the Taihu Basin, covering an area of 108 km^2 with a mean depth of 2.1 m. The lake exhibits a unique tripartite structure comprising the western (area: 33 km^2), central (area: 33 km^2), and eastern (area: 42 km^2) sectors. Water quality exhibits a spatial gradient, improving from west to east driven by the distribution of nutrient-rich inflows. In contrast, DTH (31°03′ N, 120°28′ E), located in the southeast corner of Lake Taihu, is shallower (mean depth: 1.3 m) and has served as an extensive aquaculture zone (106 km^2) since 1984. Both ecosystems experienced comparable climatic conditions during the study period. Mean air temperature and annual precipitation were 17.1 °C and 1125 mm in LYC, and 17.5 °C and 1112 mm in DTH, respectively.

Both LYC and DTH are prominent crab farming sites in the YRD region. LYC primarily practices monoculture of Chinese mitten crabs (CMC), whereas DTH employs a polyculture model, rearing CMC alongside shrimp and fish. Both systems follow similar management protocols, including pre-season lime application (500–1000 kg ha^{-1}) for water quality regulation and the transplantation of submerged macrophytes to provide shelter and food for the crabs. Feed inputs, comprising artificial pellets, corn, and animal-based feed (e.g., small fish and snails), were applied from February to November. Annual feed application rates were approximately 4800 and 6400 kg C ha^{-1} yr^{-1} at the LYC and DTH sites, respectively. Detailed descriptions of the farming methodologies can be found in Liu et al. (2019) for LYC and Pu et al. (2022) for DTH.

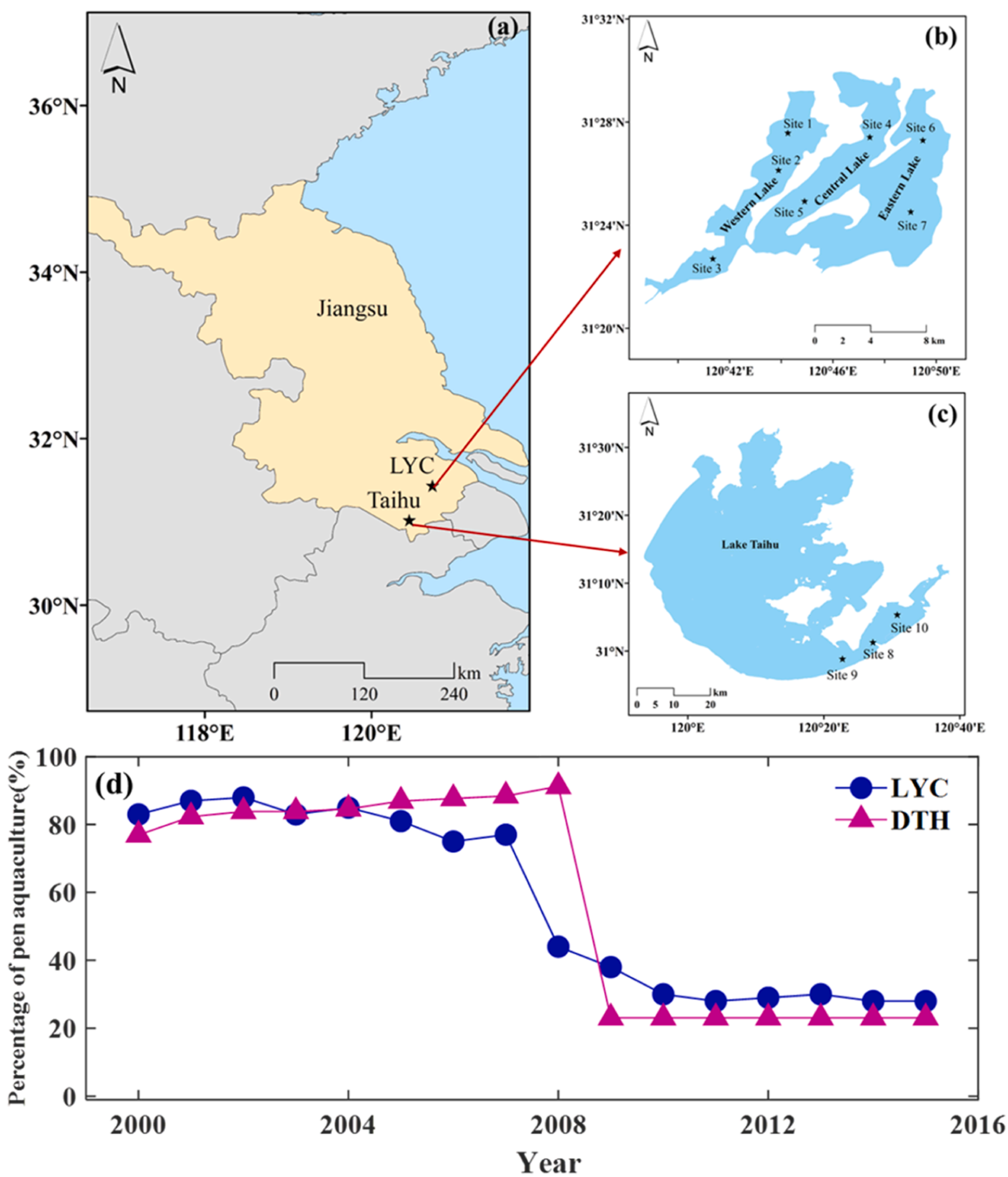

Fig. 1. (a) Distribution of LYC and DTH in China; (b and c) Distribution of sampling sites at the LYC site (Sites 1–7) and at the DTH site (Sites 8–10), respectively. (d) Interannual variation in the percentage of pen aquaculture area from 2000 to 2015 at the LYC (Blue circles) and DTH (pink triangles) sites.

2.2. Data acquisition and water sampling

Field sampling at the Lake Yangcheng (LYC) site was carried out at seven long-term monitoring sites. These sites were distributed across three lake sectors based on the spatial variability of water quality: three in the western sector (Sites 1–3), two in the central sector (Sites 4–5), and two in the eastern sector (Sites 6–7, Fig. 1). Sampling in LYC was conducted seasonally (March, August, and October) in 2000, 2003, and 2005. The sampling frequency was increased to six times annually (January, March, May, July, September, and November) from 2006 to 2011, and further intensified to monthly intervals from 2012 to 2015. Data were not available for 2001, 2002, and 2004 due to sampling gaps. To evaluate the impact of these varying sampling frequencies, a Monte Carlo-based sensitivity test was performed, which confirmed that the shifts in frequency did not compromise the robustness of the detected interannual trends (see Supplementary Text S1 and Fig. S1). In Dongtaihu Bay (DTH), three sampling sites were established (Sites 8–10; Fig. 1). Water samples were collected seasonally in February (winter), May (spring), August (summer), and November (autumn) from 2000 to 2015 at Site 8, and from 2005 to 2015 at Sites 9 and 10.

Physicochemical parameters, including water temperature (T_w), alkalinity (Alk), pH, dissolved oxygen (DO), ammonium nitrogen (NH_4^+-N), total nitrogen (TN), total phosphorus (TP), and chlorophyll a (Chl-a), were measured following standard protocols. In brief, T_w, DO, and pH were measured in situ using multiparameter probes. Subsurface water samples (0.5 m depth) were collected and stored in coolers for laboratory analysis. Alk was determined via Gran titration with a precision of ± 0.5 %. TN and TP analyses followed national standards (GB11894–89 and GB11893–89, respectively) using persulfate digestion and spectrophotometry. NH_4^+-N concentration was determined by the indophenol blue method, and Chl-a concentrations were determined spectrophotometrically after hot ethanol extraction. For the LYC dataset, missing Alk values were interpolated or imputed from mean and measured environmental variables (see Supplementary Text S2). At the DTH site, long-term water sampling and laboratory analyses were conducted by the Taihu Laboratory for Lake Ecosystem Research (TLLER).

At the LYC site, the pen aquaculture area was extracted from Landsat imagery using the automated classification method developed by Luo et al. (2020), which achieved an overall accuracy exceeding 92 %. For DTH, aquaculture spatial data were obtained from the analysis by Li et al. (2023), who employed a similar remote sensing-based classification framework. To evaluate the dynamics of aquatic vegetation and its potential for carbon sequestration, the Normalized Difference Vegetation Index (NDVI) and Gross Primary Production (GPP) were employed as key indicators (Luo et al., 2016; Hao et al., 2025). Monthly NDVI data were derived from 30-m resolution Landsat imagery processed via the Google Earth Engine (GEE) platform to track the spatial and temporal variations in macrophyte coverage. Concurrently, annual GPP was estimated using a modified Vertically Generalized Production Model (VGPM). The VGPM framework has been widely validated and applied to estimate phytoplankton primary production in large shallow lakes within the Yangtze River basin, demonstrating high reliability in capturing regional carbon fixation patterns (Deng et al., 2017; Jia et al., 2020; Hao et al., 2025). This model was driven by a combination of long-term in situ water quality observations and satellite-derived environmental forcing, providing a robust measure of the system's photosynthetic carbon fixation capacity (see Supplementary Text S3 for detailed parameterization and model description).

2.3. Calculations

The partial pressure of CO_2 (pCO_2, μatm) was computed based on carbonate system thermodynamics using in situ measurements of water temperature, pH, and alkalinity, following calculation protocols detailed in prior literature (Raymond et al., 2013; Abril et al., 2015; Xiao et al., 2020, 2024b). Given the use of interpolated/imputed alkalinity for the historical LYC dataset, a Monte Carlo sensitivity analysis was performed to evaluate potential uncertainties (see Supplementary Text S2). We utilized the long-term observational dataset from the adjacent DTH to constrain the seasonal variability parameters for the simulation. The results suggested that pCO_2 estimates were robust to alkalinity fluctuations, with a mean relative error of ~ 12 %. In contrast, the estimates exhibited high sensitivity to pH variations. Given that pH was measured in situ with high precision, this confirms that the derived pCO_2 dynamics were reliable (Fig. S2).

The CO_2 exchange flux (F_c, g C m^{-2}d^{-1}) across the water-air interface was estimated using the thin boundary layer model (Cole and Caraco, 1998), expressed as:

$$F_c = 0.044 \times k \times K_H \times (pCO_2 - p_a)$$

Where k (m d^{-1}) represents the gas transfer coefficient of CO_2 derived from standard wind-speed dependent models (Cole and Caraco, 1998). The wind-based model by Cole and Caraco (1998) was selected because our prior comparative analysis in this region demonstrated that its annual flux estimates were nearly identical to those derived from complex convection-based models (Xiao et al., 2017). This model selection ensures consistency across the multidecadal dataset for robust interannual comparisons. K_H (mol L^{-1} atm^{-1}) denotes the temperature-dependent solubility of CO_2 (Henry's law constant); and p_a (μatm) is the atmospheric CO_2 partial pressure, monitored via a high-precision gas analyzer (precision: 0.05 μatm; Xiao et al., 2014). 0.044 is a conversion factor. A positive F_c (CO_2 flux) value indicates a net CO_2 efflux from the water to the atmosphere. Full calculation procedures are available in Xiao et al. (2020).

To characterize the metabolic balance of the lake, dissolved oxygen saturation (S_{do}) was utilized as a proxy (Brigham et al., 2019). S_{do} is defined as the ratio of observed dissolved oxygen concentration to the saturation concentration at the specific water temperature. Generally, $S_{do} > 1$ reflects dominant photosynthetic oxygen production (CO_2 sink), while $S_{do} < 1$ suggests dominant respiratory oxygen consumption (CO_2 source).

2.4. Data analysis

2.4.1. Data processing

To characterize spatial heterogeneity, LYC was partitioned into three sectors: western (Sites 1–3), central (Sites 4–5), and eastern (Sites 6–7). For spatial analysis, data from individual sites within each sector were spatially averaged to obtain zonal-specific values. To assess temporal trends (e.g., seasonal and inter-annual variations), measurements from all sampling sites were spatially averaged for each sampling campaign to represent the whole-lake condition. Seasons were defined as spring (March–May), summer (June–August), autumn (September–November), and winter (December to February). Annual means were calculated based on the monthly or seasonal time series from 2000 to 2015. All data processing and visualization were performed using MATLAB (MathWorks, Inc., Natick, MA, USA).

2.4.2. Statistical and machine learning analysis

To disentangle the complex environmental drivers regulating pCO_2 dynamics, we adopted a complementary framework combining traditional statistical approaches with machine learning techniques. First, simple linear regression and Pearson correlation analyses were applied to determine the directionality (positive or negative) and strength of linear associations between pCO_2 and environmental parameters. Subsequently, the Random Forest (RF) algorithm was employed to identify key predictors and capture potential non-linear interactions that might be overlooked by linear models. We selected this model due to its known robustness against overfitting and multicollinearity in complex ecological datasets (Kim et al., 2020; Martinsen et al., 2020).

The RF models were constructed using the TreeBagger function in

MATLAB. The dataset was randomly partitioned into training (70 %) and testing (30 %) subsets. Predictor variables included water temperature (T_w), dissolved oxygen (DO), ammonium nitrogen (NH_4^+-N), total nitrogen (TN), total phosphorus (TP), chlorophyll a (Chl-a), air temperature (T_a), wind speed (WS), NDVI, and the proportional area of pen aquaculture (Area). Hyperparameters were optimized based on out-of-bag (OOB) error minimization. Variable importance was quantified using the increase in mean squared error, which measures the decrease in model predictive accuracy when a specific predictor's values are randomly permuted (Shi et al., 2023). Model accuracy was quantified using the root mean squared error (RMSE), the coefficient of determination (R^2), and the index of agreement (IOA).

3. Results

3.1. Variability of pen aquaculture area, meteorological conditions, and biochemical variables

The temporal evolution of pen aquaculture area exhibited distinct patterns between LYC and DTH from 2000 to 2015 (Fig. 1). In LYC, sectoral analysis revealed marked spatial heterogeneity: the western sector maintained 88 % coverage until its complete removal in 2008, whereas the eastern and central sectors showed progressive declines with differing transition years (Fig. S4). Overall, the trajectory of LYC can be categorized into three stages: (1) Stage I (2000–2007) featured a gradual decline from 83 % to 76 % coverage, reflecting a period of still-intensive farming practices; (2) Stage II (2008–2010) showed an abrupt reduction from 65 % to 28 % due to the rigorous implementation of the "pen aquaculture retreat" policy; and (3) Stage III (2011–2015) stabilized at approximately 28 %, indicating a new equilibrium in aquaculture area management. When applying this LYC-based temporal framework to DTH, a distinct divergence was observed during the early phase. In contrast to the decline in LYC, DTH displayed an inverse trajectory during Stage I, expanding from 77 % to 90 % coverage. However, the trends converged in Stage II, where DTH also experienced a sharp contraction (dropping to 23 %), followed by stabilization in Stage III. The 16-year period from 2000 to 2015 was selected as the core analysis window to ensure strict temporal consistency for the comparative assessment of both lake systems. Crucially, this duration captures the full ecological response to the initial "partial retreat" policy, effectively isolating these legacy effects from the distinct "complete ban" phase implemented post-2018 (Fig. S4).

In terms of meteorological conditions (2000–2015), both lakes exhibited synchronized interannual trends characterized by slight warming and declining wind speed (Fig. 2a, b). Linear regression analysis indicated a significant downward trend in wind speed for both sites (rates of decline: 0.05 m s^{-1} yr^{-1} for LYC and 0.03 m s^{-1} yr^{-1} for DTH, $p < 0.001$). Regarding air temperature, although both lakes showed an

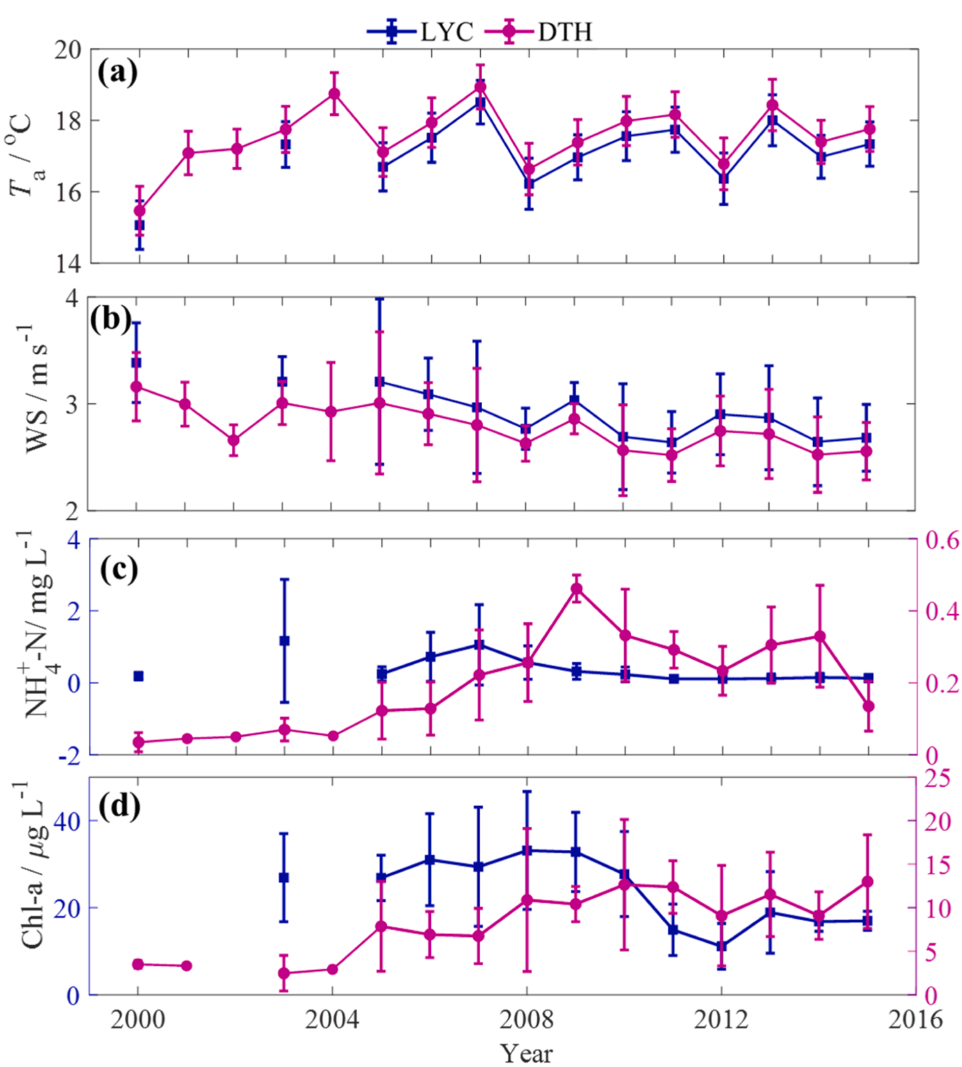

Fig. 2. Interannual variation in (a) air temperature (T_a), (b) wind speed (WS), (c) NH_4^+-N concentration, and (d) Chl-a concentration at the LYC and DTH sites from 2000 to 2015. The error bars indicate standard error.

increasing tendency (LYC: 0.08 °C yr^{-1}; DTH: 0.06 °C yr^{-1}), these trends were not statistically significant (p > 0.05). Despite these subtle temporal shifts, the overall magnitudes remained comparable between the two sites (LYC: 17.1 °C, 2.9 m s^{-1}; DTH: 17.5 °C, 2.8 m s^{-1}) (Fig. 2a, b; Table 1).

In contrast to the uniform meteorological conditions, biochemical variables exhibited marked spatiotemporal heterogeneity. Spatially, LYC maintained significantly elevated nutrient concentrations, with annual means 2–3 times higher than those of DTH (NH_4^+-N: 0.42 vs. 0.23 mg L^{-1}; Chl-a: 25 vs. 9 μg L^{-1}, Fig. 2c, d, Table 1). Within LYC, a distinct decreasing west-to-east gradient was observed, despite consistent seasonal patterns (Fig. S5). Specifically, concentrations peaked in the western sector due to nutrient-rich inflows, transitioned to intermediate levels in the central sector, and reached their lowest values in the east. Temporally, however, the two lakes exhibited diverging trajectories. Interannual dynamics in LYC closely mirrored aquaculture phase changes: Stage I (2000–2007) showed stable elevated levels; Stage II (2008–2010) featured dramatic declines, including a notable 78 % reduction in NH_4^+-N during the intensive removal period; and Stage III (post–2010) maintained a new equilibrium with lower concentrations. Conversely, DTH exhibited gradual nutrient increases throughout the study period. Notably, policy implementation in LYC drove significant water quality improvements from 2000 to 2015, resulting in reductions of 44 % for TN, 54 % for TP, 30 % for NH_4^+-N, and 37 % for Chl-a, alongside a 6 % increase in DO.

3.2. Temporal dynamics of pCO_2

Substantial inter-annual variability in pCO_2 was observed in both lake systems over the 16-year study period (Fig. 3a). Overall, LYC exhibited significantly wider fluctuations and higher levels compared to DTH. Annual pCO_2 in LYC ranged from 540 μatm in 2010 to 1640 μatm in 2006, yielding a long-term mean of 1180 ± 390 μatm (Table S1). In comparison, DTH showed narrower variability (370–1180 μatm) and a significantly lower mean of 716 ± 185 μatm. The temporal dynamics of pCO_2 in both lakes evolved through three distinct stages, yet displayed diverging trajectories. During Stage I (2000–2007), LYC maintained high saturation levels (Mean: 1435 μatm) consistent with intensive farming, whereas DTH started at a much lower baseline but exhibited an increasing trend (Mean: 617 μatm). A sharp divergence occurred in Stage II (2008–2010): LYC experienced a drastic decline to a mean of 870 μatm following intensive aquaculture retreat, while DTH continued to rise, reaching its peak phase average of 951 μatm. By Stage III (2011–2015), LYC stabilized with a moderate rebound (Mean: 1195 μatm), while DTH levels decreased to a lower equilibrium (Mean: 732 μatm). With the exception of the intensive removal phase (Stage II), mean pCO_2 values in LYC remained higher than those in DTH, highlighting the persistent footprint of higher historical aquaculture intensity.

Regarding seasonal dynamics, distinct patterns were observed despite the lack of statistically significant differences (p > 0.05) at either site (Fig. 4a; Table S1). In LYC, seasonal mean pCO_2 peaked in autumn (1332 ± 430 μatm), followed by summer (1143 ± 940 μatm), spring (938 ± 329 μatm), and winter (910 ± 308 μatm). In contrast, DTH displayed an inverse pattern, with higher values during colder seasons (autumn: 761 ± 215 μatm; winter: 794 ± 234 μatm) compared to warmer periods (spring: 662 ± 310 μatm; summer: 646 ± 360 μatm). However, cross-comparison revealed that these seasonal variations were secondary to the dominant inter-annual trends driven by anthropogenic interventions.

3.3. Spatial heterogeneity and sector-specific responses in LYC

Spatially, LYC exhibited a pronounced decreasing west-to-east pCO_2 gradient across all three stages, consistently matching the historical distribution of aquaculture intensity (Fig. S6, Table 1). The highest concentrations were observed in the nutrient-rich western sector (1490 ± 538 μatm), transitioning to intermediate levels in the central sector (1200 ± 547 μatm) and the lowest values in the eastern sector (860 ± 365 μatm).

We further decoupled the temporal evolution for each specific sector to examine their distinct trajectories under varying aquaculture removal timelines (Fig. S6). During the intensive retreat period (Stage I to Stage II), all sectors exhibited consistent declines, yet the magnitude of response was closely coupled with the intensity of aquaculture retreat in each zone. The western sector, which underwent the most radical change with complete aquaculture removal in 2008, showed the sharpest response with a 53 % reduction in pCO_2 (from 1853 to 880 μatm, Table 1). This synchronous decline across sectors indicates that aquaculture reduction played a dominant role in carbon mitigation during the early restoration phase. However, trends diverged notably in the post-restoration phase (Stage III). While the eastern sector stabilized at a low-carbon equilibrium (~ 810 μatm), comparable to its Stage II level (~ 815 μatm), the western and central sectors exhibited a significant "V-shaped" rebound. Notably, this rebound occurred in the western sector despite the complete elimination of aquaculture (0 % coverage). This spatial divergence highlights that long-term carbon dynamics in the western region remain unstable compared to the resilient recovery observed in the east.

3.4. CO_2 flux estimate

Consistent with pCO_2 measurements, both lake aquaculture systems acted as net atmospheric CO_2 sources (Fig. 3b and 4 b; Table 1 and S1),

Table 1
Mean values of key environmental variables, pCO_2, and CO_2 fluxes across lake sectors at the LYC and DTH sites during different management stages.

Stage	Lake	Key Environmental factors										
		T_a / °C	WS / m s^{-1}	T_W / °C	TN / mg L^{-1}	TP/ mg L^{-1}	NH_4^+-N/ mg L^{-1}	Chl-a/ μg L^{-1}	DO / mg L^{-1}	pH	pCO_2 / μatm	F_c / g m^{-2}d^{-1}
Stage I	West	17.0	3.17	19.3	2.92	0.10	0.98	29	8.75	8.06	1853	2.08
	Central	17.0	3.17	19.6	2.47	0.09	0.68	30	9.43	8.23	1415	1.42
	East	17.0	3.17	19.6	2.42	0.08	0.64	28	9.85	8.35	1036	0.91
	Whole	17.0	3.17	19.5	2.60	0.09	0.77	29	9.34	8.21	1435	1.47
	DTH	17.5	2.93	18.3	0.99	0.06	0.09	4.8	9.03	8.15	617	0.26
Stage II	West	16.9	2.83	18.6	2.30	0.11	0.48	38	9.75	8.42	880	0.67
	Central	16.9	2.83	18.6	1.96	0.09	0.34	31	9.47	8.39	914	0.71
	East	16.9	2.83	18.5	1.54	0.06	0.28	24	9.60	8.39	815	0.57
	Whole	16.9	2.83	18.6	1.94	0.09	0.37	31	9.60	8.40	870	0.65
	DTH	17.3	2.69	18.1	1.59	0.06	0.35	11	9.29	8.06	951	0.66
Stage III	West	17.3	2.75	18.6	1.97	0.08	0.17	15	9.54	8.12	1577	1.52
	Central	17.3	2.75	18.5	1.35	0.06	0.11	17	9.68	8.16	1197	1.01
	East	17.3	2.75	18.8	1.09	0.04	0.11	14	10.33	8.36	809	0.48
	Whole	17.3	2.75	18.6	1.47	0.06	0.13	15	9.85	8.21	1195	1.01
	DTH	17.7	2.61	18.3	1.30	0.05	0.26	11	8.76	9.16	732	0.37

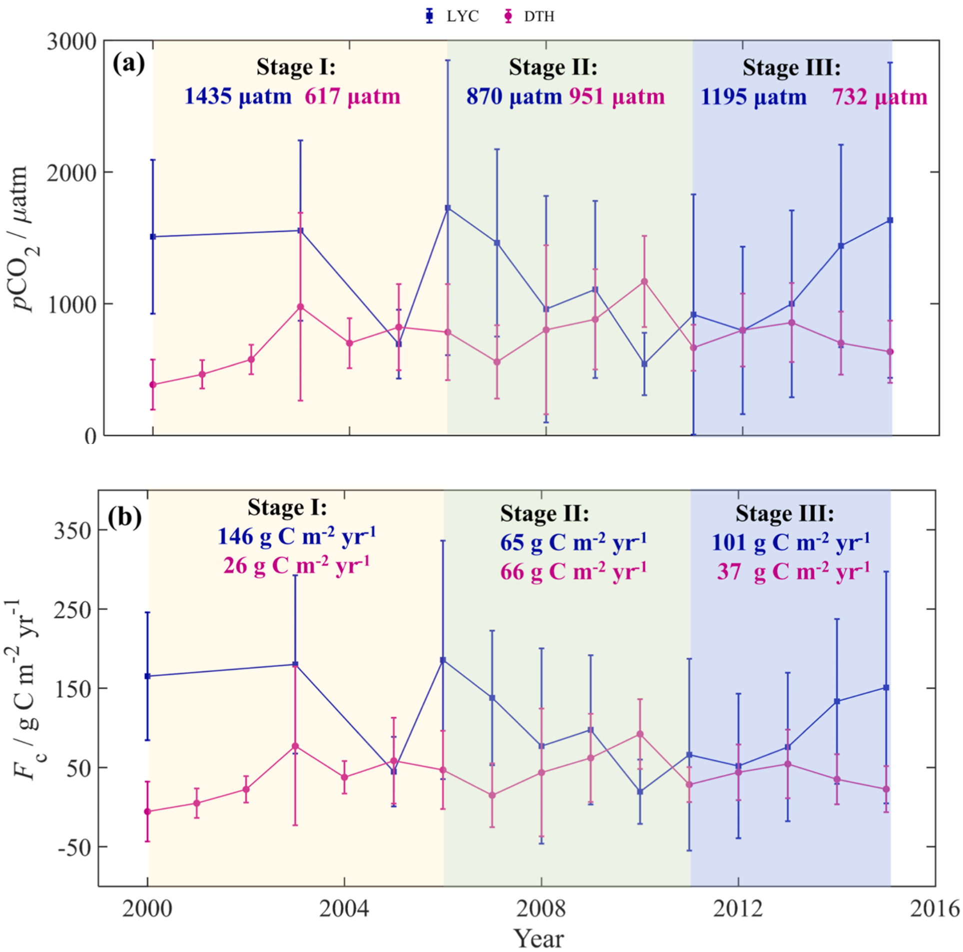

Fig. 3. Interannual variation in (a) pCO_2 (µatm) and (b) F_c (g C m^{-2} yr^{-1}) at the LYC and DTH sites from 2000 to 2015.

though with distinct emission magnitudes. LYC functioned as a significant emitter with an annual mean of 108 g C m^{-2} yr^{-1}, approximately threefold higher than that of DTH (37 g C m^{-2} yr^{-1}). Interannual variability was substantial for both sites (Fig. 3b). Annual fluxes in LYC fluctuated widely, ranging from 19 g C m^{-2} yr^{-1} in 2010 to 181 g C m^{-2} yr^{-1} in 2003. In comparison, DTH exhibited lower fluxes, ranging from -6 g C m^{-2} yr^{-1} in 2000 to 93 g C m^{-2} yr^{-1} in 2010. Across the three development stages, flux dynamics closely tracked the pCO_2 trends described above, with LYC maintaining consistently higher fluxes than DTH across all corresponding phases despite their respective fluctuations.

Spatially and seasonally, CO_2 fluxes followed patterns consistent with pCO_2 distributions (Fig. 4b). Spatially, LYC exhibited a pronounced decreasing west-to-east gradient, with the western sector recording the highest emissions (0.41 ± 0.20 g C m^{-2} d^{-1}), followed by the central (0.29 ± 0.21 g C m^{-2} d^{-1}) and eastern sectors (0.17 ± 0.15 g C m^{-2} d^{-1}). Seasonally, LYC emissions peaked in summer (0.38 ± 0.26 g C m^{-2} d^{-1}), whereas DTH fluxes were highest in winter (0.14 ± 0.08 g C m^{-2} d^{-1}), although these seasonal differences were not statistically significant at either site ($p > 0.05$).

3.5. Factors influencing the pCO_2 variability

Long-term measurements revealed distinct regulatory patterns of pCO_2 variability in the two lake systems. Correlation analysis identified nutrient loadings and S_{do} as the most consistent predictors (Fig. 5; Table 2). At both LYC and DTH, pCO_2 exhibited consistent significant positive correlations with nutrient parameters including NH_4^+-N and TN across most seasons (Table 2), with correlation coefficients ranging from 0.15 to 0.77 ($p < 0.05$). Conversely, S_{do} showed a strong negative correlation with pCO_2 particularly in spring (LYC: $r = -0.72$; DTH: $r = -0.50$, $p < 0.05$), reflecting a strong coupling between dissolved gas saturation and water quality status. In contrast, climatic factors (air temperature and wind speed) showed weak or sporadic associations with pCO_2, suggesting they played a secondary role compared to water quality parameters.

Regarding biological drivers, seasonal analyses indicated a general decoupling between primary production proxies and pCO_2. On an annual scale, neither Chl-a nor NDVI showed significant correlations with pCO_2 at either site ($p > 0.05$). Although a notable exception was observed in summer in LYC where NDVI showed a significant negative correlation ($r = -0.46$), the overall lack of correlation implies that the signal of photosynthetic uptake was largely overwhelmed by intense system-wide respiration. Notably, the response to water temperature diverged significantly between the two lakes. pCO_2 in LYC showed a positive correlation with T_w ($r = 0.12$, $p < 0.05$), consistent with respiration-dominated processes. Conversely, DTH exhibited a negative relationship ($r = -0.16$, $p < 0.05$).

3.6. Predictive model performance

The Random Forest (RF) model further elucidated the hierarchy of key drivers regarding pCO_2 variability and established predictive frameworks for both lake systems. Analysis of variable importance rankings, quantified by the percentage increase in mean squared error (%IncMSE), revealed distinct top-tier predictors for each system (Fig. 6a and b). For LYC, aquaculture area, DO, and NH_4^+-N emerged as the predominant predictors, exerting the most substantial influence on

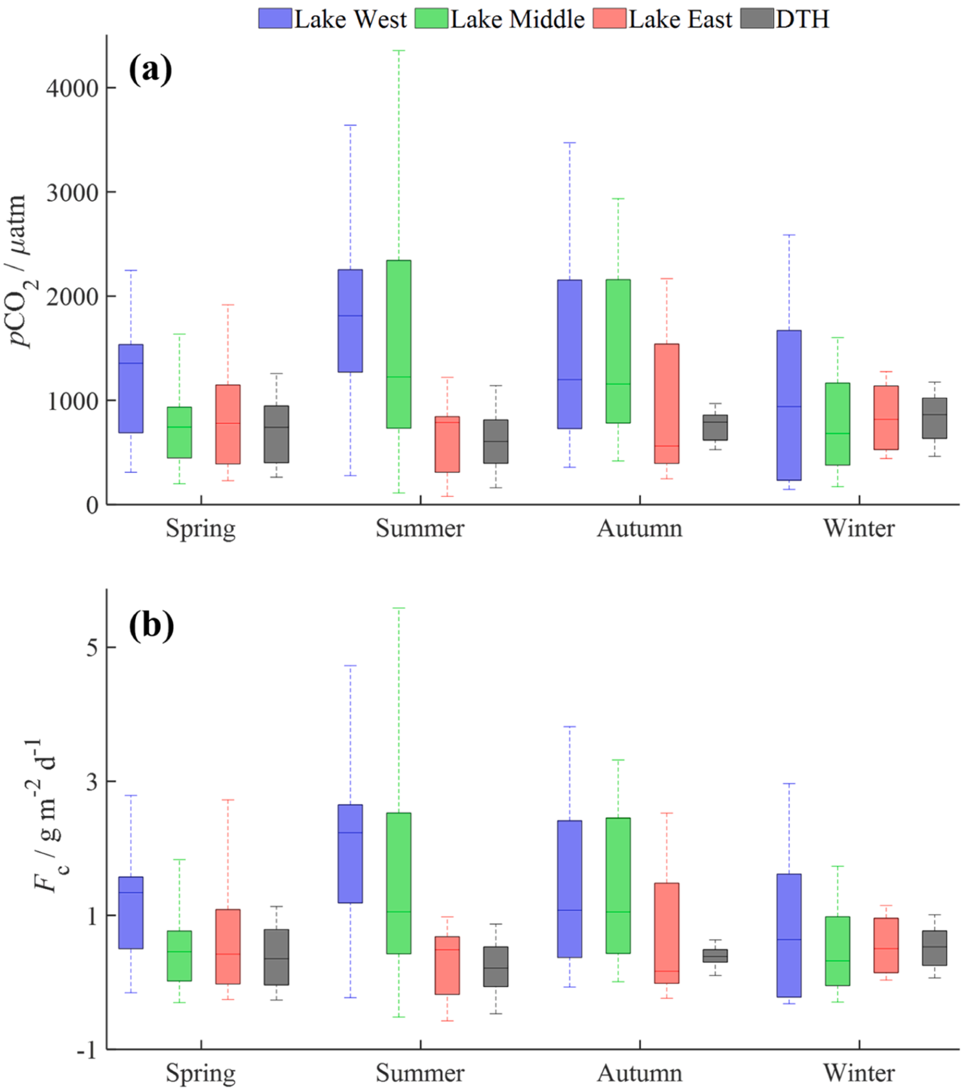

Fig. 4. Seasonal variation in (a) pCO_2 (μatm) and (b) F_c (g m^{-2}d^{-1}) at the LYC and DTH sites from 2000 to 2015.

model predictive accuracy compared to other environmental variables (Fig. 6a). For DTH, TP and NH_4^+-N were identified as the primary driver, followed by aquaculture area (Fig. 6b). These findings corroborate the linear associations observed in the regression analysis (Section 3.5) by confirming the critical role of nutrients and DO, while further uncovering the non-linear influence of aquaculture area, a factor that linear models failed to fully capture.

Using these predictor variables, the performance of the RF-based pCO_2 predictions exhibited a marked contrast between the two systems (Fig. 6c and d). For LYC, the model demonstrated satisfactory predictive accuracy, with simulated values closely clustering around the 1:1 line for both training ($R^2 = 0.86$, IOA = 0.93, RMSE = 395 μatm) and testing sets ($R^2 = 0.71$, IOA = 0.81, RMSE = 475 μatm). However, a slight underestimation occurred in the high pCO_2 range. In contrast, the model performance for DTH was more limited, characterized by greater scatter and lower explanatory power in the testing set ($R^2 = 0.34$, IOA = 0.74, RMSE = 274 μatm). This disparity likely reflects the inherent complexity of the semi-enclosed DTH system, where unmeasured physical or hydrological factors may exert a stronger stochastic influence than in LYC.

4. Discussion

4.1. Lake aquaculture as sustained net CO_2 sources

Aquaculture serves as a vital source of protein and economic livelihood, yet whether it acts as a net CO_2 source or sink in the carbon cycle remains a subject of debate (Kosten et al., 2020; Chen et al., 2023). Despite this ongoing debate, research has predominantly focused on closed pond systems, leaving open lake-based pen aquaculture comparatively understudied (Xiao et al., 2024b; Zhao et al., 2025). Addressing this critical knowledge gap, our 16-year dataset provides robust evidence that both LYC and DTH consistently functioned as net CO_2 sources, with mean annual emissions of 108 ± 56 and 37 ± 24 g C m^{-2} yr^{-1}, respectively. These findings align with the recent global assessment by Zhang et al. (2026a), which synthesized over 2000 measurements and reported that 77 % of aquaculture CO_2 fluxes were positive, confirming the sector's predominant role as an atmospheric source. Our observed values fall within the range (26–110 g C m^{-2} yr^{-1}) reported for other inland aquaculture systems in China (Yang et al., 2018; Yuan et al., 2019; Zhang et al., 2022a, b). Notably, the emission intensity in LYC was comparable to regional natural lakes (~ 93 g C m^{-2} yr^{-1}; Li et al., 2018), whereas emissions in DTH were substantially lower. These results confirm that lake aquaculture systems act as significant carbon sources, yet their emission magnitudes are strongly regulated by

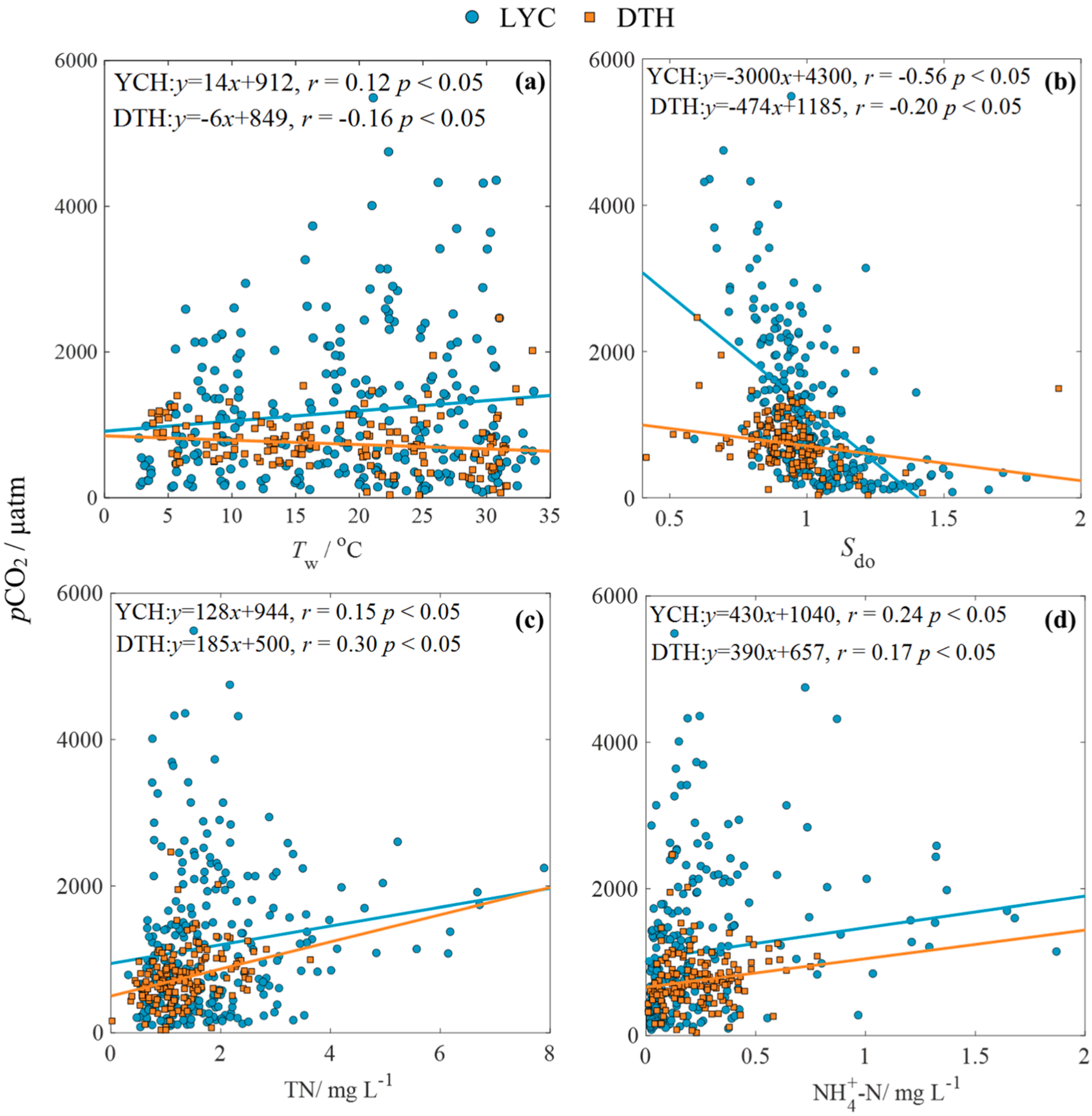

Fig. 5. Relationship between the mean lake pCO_2 at the LYC and DTH sites and (a) water temperature (T_w), (b) DO saturation concentration (S_{do}), (c) TN concentration, and (d) NH_4^+-N concentration.

Table 2
Relationships between pCO_2 and key aquatic environmental variables in different seasons from 2000 to 2015 at the LYC and DTH sites.

Season	Site	T_a	WS	T_w	DO	S_{do}	NH_4^+-N	TN	TP	Chl-a	NDVI
Spring	LYC	−0.36	0.36	−0.34 **	−0.33*	−0.72**	0.77**	0.73 *	0.54 **	0.22	−0.12
	DTH	−0.31	0.19	0.06	−0.50 **	−0.50 **	0.04	0.50**	0.20	0.22	0.04
Summer	LYC	−0.006	0.18	−0.14	−0.66**	−0.66**	0.31*	0.33 *	0.42**	−0.28	−0.46*
	DTH	0.24	−0.27	0.13	−0.14	−0.10	−0.15	0.26	−0.19	−0.11	−0.03
Autumn	LYC	−0.07	0.02	−0.29	−0.46 **	−0.52 **	0.44 **	0.37 *	0.44 **	−0.15	−0.18
	DTH	−0.29	0.36**	−0.44*	−0.07	−0.34*	0.39 *	0.39 *	0.38 *	0.15	−0.21
Winter	LYC	−0.07	0.02	0.38	−0.48**	−0.24	0.70 **	0.52**	0.17	0.07	−0.14
	DTH	−0.39*	0.31	−0.15	−0.01	−0.19	0.49 **	0.27	0.17	−0.06	0.25
Overall	LYC	0.15	0.09	0.12*	−0.51**	−0.56**	0.24 **	0.15*	0.31**	−0.08	−0.13
	DTH	−0.15	−0.02	−0.16*	−0.02	−0.20*	0.17**	0.30*	−0.03	−0.02	−0.06

* Correlation is significant at the 0.05 level.
** Correlation is significant at the 0.001 level.

management intensity, underscoring the crucial need to incorporate these systems into global carbon budget assessments (Zhang et al., 2026a).

Crucially, our long-term results challenge the initial hypothesis that aquaculture retreat triggers a linear, continuous decline in CO_2 emissions. While previous studies in urban lakes suggested that management-driven nutrient reduction leads to a monotonic decrease in pCO_2 (Xiao et al., 2020, 2023), LYC exhibited a striking non-linear "V-shaped" trajectory. Emissions dropped sharply by 54 % during the intensive removal phase but unexpectedly rebounded in the

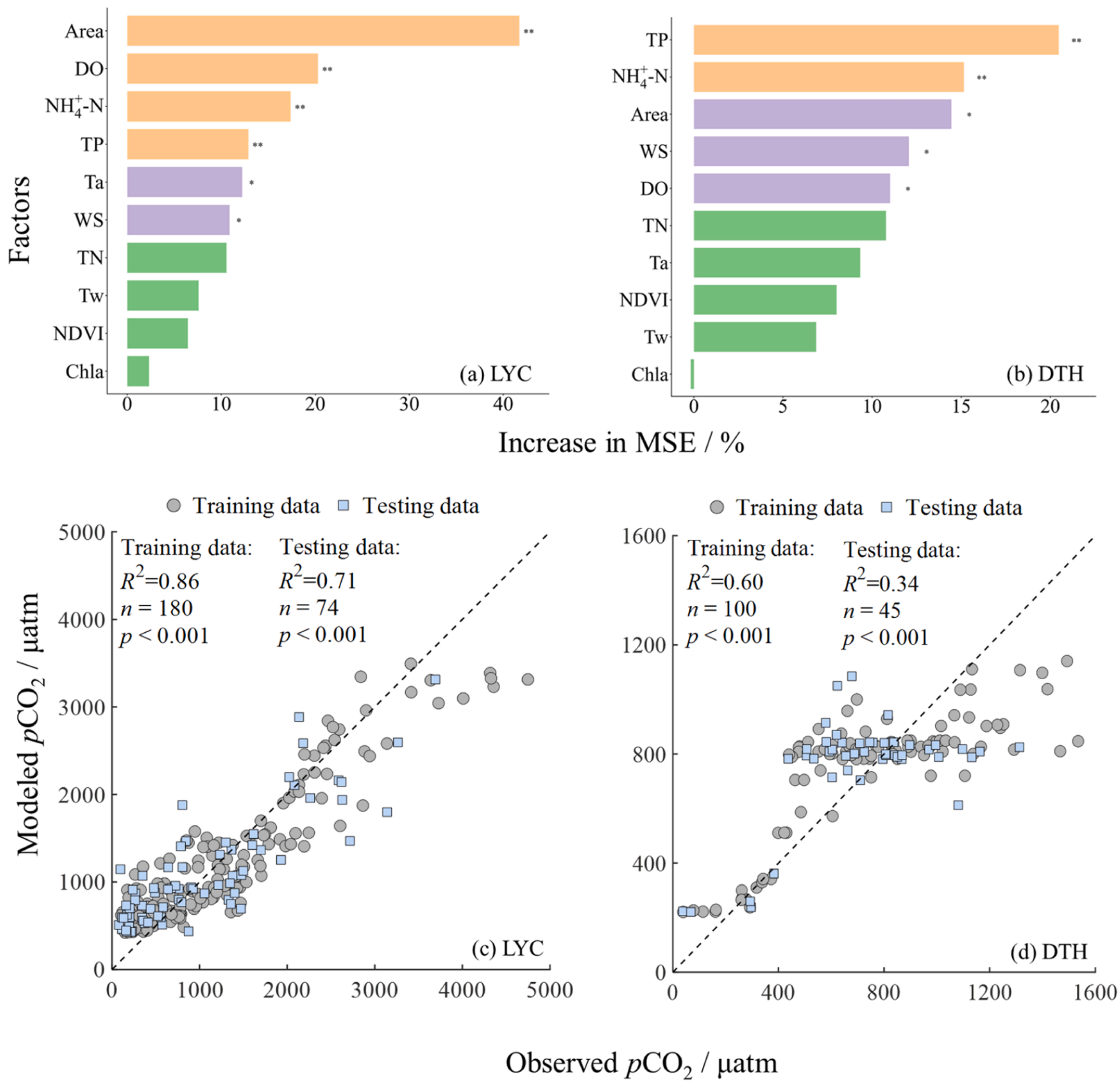

Fig. 6. Variable importance in the Random Forest model at the LYC (a) and DTH (b) sites, respectively; Performance of the final RF model on the training and testing data at the LYC (c) and DTH (d) sites, respectively. The dotted line is a 1:1 relationship.

post-restoration phase. This divergence highlights the distinct "hysteresis effect" of aquaculture systems compared to general eutrophic lakes (Jeppesen et al., 2007), confirming that the recovery path in these highly disturbed environments does not simply mirror their degradation trajectories. In sharp contrast, DTH maintained a lower, stable equilibrium throughout the same period. This stability is robustly corroborated by our extended observations in DTH from 2016 to 2020 (Fig. S7), confirming that the gradual, phased retreat strategy avoided the drastic regime shift observed in LYC. This comparison also validates the necessity of long-term monitoring. A short-term study (< 2 years) conducted during Stage II would have erroneously concluded that retreat solves the carbon problem, completely missing the subsequent rebound. This highlights the importance of decadal-scale datasets to obtain critical insight and unbiased results.

4.2. Potential drivers of CO_2 dynamics across lake aquaculture system

Nutrient availability serves as the fundamental regulator of carbon emission magnitudes across the studied aquaculture systems. The annual CO_2 flux in LYC was approximately threefold higher than that in DTH, a disparity that aligns with the substantial differences in their trophic status rather than meteorological conditions (Section 3.1). TN and NH_4^+-N concentrations, proxies for anthropogenic loading, were 24 % and 45 % higher in LYC than those in DTH, respectively, and exhibited significant positive correlations with pCO_2 in both systems ($p < 0.05$; Fig. 5; Table 2). This nutrient-CO_2 relationship is consistent with findings in other aquaculture systems, where elevated external inputs stimulate the heterotrophic degradation of organic carbon, thereby enhancing respiratory CO_2 production (Maberly et al., 2013; Xiao et al., 2020; Zhang et al., 2022b, 2024b; Yang et al., 2024; Zhao et al., 2025). Furthermore, nutrient variability effectively explains the initial emission decline in LYC: the substantial 54 % reduction in CO_2 emissions from Stage I to Stage II coincided with sharp declines in TN (26 %) and NH_4^+-N concentrations (52 %) following the intensive pen removal.

However, despite continued declines in nutrient concentrations, the "V-shaped" rebound in Stage III suggests a fundamental decoupling between external loading and carbon emissions. While sediment mineralization is typically identified as a primary internal carbon source in shallow lakes (Gudasz et al., 2010; Hall et al., 2019; Jongejans et al., 2021), the intensive sediment dredging, typically involving ∼ 30 cm, implemented during this phase alters this expectation. Since this intervention physically stripped the active surface layer richest in labile organic carbon, it theoretically reduced the sediment carbon supply (Chen et al., 2021; Nijman et al., 2022; Liu et al., 2024b; Hao et al., 2025). Consequently, the sediment-to-water carbon flux during Stage III is expected to be marginalized rather than enhanced. Given the suppression of sediment fluxes, the metabolic balance between water column photosynthesis and respiration emerges as the dominant regulator of ecosystem CO_2 dynamics (Del Giorgio and Williams, 2005; Chmiel et al., 2016; Gao et al., 2021;Jia et al., 2023). Applying this framework to LYC, we attribute the Stage III pCO_2 surge to a severe imbalance in water column metabolism, specifically the synergy between "autotrophic sink collapse" and "warming-enhanced respiration". The aggressive dredging inadvertently eliminated the ecosystem's biological buffers (macrophytes and algae), which serve as critical regulators of carbon dynamics (Pu et al., 2022; Hong et al., 2025). This loss is evidenced by the sharp reversal in ecosystem productivity: while the initial recovery in Stage II saw GPP rise to 750 g C m^{-2} yr^{-1}, Stage III experienced a drastic 37 % collapse (plummeting to 474 g C m^{-2} yr^{-1}), accompanied by a marked loss in vegetation cover (NDVI dropping from 0.010 to −0.045) (Fig. S3). Consequently, this underscores a pivotal lesson for ecological restoration: effective strategies must strike a delicate balance between eliminating sediment-borne pollution and preserving the structural integrity of the macrophyte community.

Crucially, the divergent temperature-pCO_2 relationships between the two lakes provide corroborative evidence for this metabolic shift (Fig. 5a; Table 2). In LYC, the observed positive correlation between water temperature and pCO_2 suggested that the systems were dominated by heterotrophy. Lacking the buffering capacity of submerged vegetation, rising temperatures may stimulate microbial respiration, a universal thermodynamic response described by metabolic theory (Gudasz et al., 2010; Yvon-Durocher et al., 2012, 2017). Consequently, emissions were driven by thermal stimulation, leading to peak values during the warm summer and autumn seasons. In sharp contrast, DTH exhibited a negative temperature-pCO_2 correlation, a pattern characteristic of healthy macrophyte-dominated lakes (Kosten et al., 2010; Natchimuthu et al., 2014). In this system, warmer temperatures during the growing season stimulated photosynthetic uptake rates that exceeded respiratory releases, resulting in CO_2 depletion in summer and accumulation only during the winter senescence phase. To fully resolve these mechanisms, future research should integrate high-frequency monitoring of sediment-water interface fluxes with water column metabolic dynamics to quantitatively disentangle the relative contributions of these distinct carbon sources.

4.3. Implications and perspectives

Regional-to-global CO_2 emissions from aquaculture have been estimated using bottom-up approaches that multiply areal extent by a fixed emission factor (Yuan et al., 2019; Dong et al., 2022; Zhang et al., 2026a). Although significant efforts have been made to refine these factors across various aquaculture systems and species (e.g., Chen et al., 2016; Yang et al., 2018; Zhang et al., 2022b; Chen et al., 2023; Zhao et al., 2025), most assessments rely on short-term measurements. This snapshot approach represents a critical blind spot, as aquaculture systems exhibit substantial legacy effects, where management interventions or climate-driven changes produce lagged responses detectable only through multi-year observations (Xiao et al., 2024b; Yang et al., 2024; Hong et al., 2025). Our 16-year dataset revealed pronounced interannual variations in CO_2 fluxes, with coefficients of variation reaching 190 % in LYC and 150 % in DTH. Crucially, the non-linear "V-shaped" emission trajectory observed in LYC explicitly challenges the conventional linear assumption that "removal equals reduction". These complex dynamics underscore ecosystem memory effects that static models fail to capture. We therefore emphasize the integration of long-term observational data into carbon budget frameworks to account for legacy effects and management lags, thereby supporting more accurate regional carbon assessments.

While uncertainties in areal assessment have long been considered a major source of error in emission estimates (Pi et al., 2022), a more fundamental limitation lies in the conceptual application of "area". Although remote sensing algorithms have improved the accuracy of area extraction (Liu et al., 2024a; Tong et al., 2025), most studies still treat area merely as an independent scaling factor for total emission calculations. Our long-term study challenges this static paradigm by revealing the complex dual role of aquaculture area. Notably, while conventional linear regression failed to detect straightforward relationships, our RF analysis identified area variation as a top-tier predictor of pCO_2 in both studied systems. This indicates a critical non-linear mechanism where changes in aquaculture extent directly modulate emission intensity, rather than acting solely as a multiplier. This finding parallels relationships observed in natural lake systems, where surface area fundamentally alters carbon processing rates (Kankaala et al., 2013; Holgerson and Raymond, 2016; DelSontro et al., 2018). Coupled with the recognition that human-induced changes can alter both the abundance and emission rates of inland waters (Liu et al., 2025b), our results argue that area and emission rate are not independent variables but are biogeochemically coupled. Consequently, future large-scale assessments must undergo a paradigm shift: moving beyond static scalars by integrating area as a dynamic variable that governs both the spatial extent of emissions and the biogeochemical processes determining their intensity.

4.4. Limitations

As with many other studies, this work is subject to certain limitations. First, a primary source of uncertainty arises from the indirect calculation of pCO_2 based on carbonate thermodynamics, particularly given the reliance on interpolated/imputed alkalinity for the historical LYC dataset. While this method is widely accepted in aquatic studies (e.g., Abril et al., 2015; Golub et al., 2017; Xiao et al., 2020, 2023; Hao et al., 2025), it carries inherent biases, particularly in low alkalinity/pH conditions. However, we contend that these uncertainties do not compromise our main conclusions. Our Monte Carlo sensitivity analysis (see Supplementary Text S2) quantified the potential bias, revealing a relatively low mean relative error of ~12 % attributable to alkalinity fluctuations. Crucially, the analysis confirmed that pCO_2 dynamics in these high-nutrient systems are predominantly governed by pH variability, which was measured in situ with high precision (Fig. S2; Xiao et al., 2024a). Furthermore, calculation errors are known to propagate most significantly in acidic conditions; since our samples maintained a weakly alkaline range (pH 7.51–9.28), inherent thermodynamic biases were minimized (Abril et al., 2015). Therefore, despite the indirect approach, the derived fluxes provide a robust representation of the decadal trends.

Second, the restriction of sampling to daylight hours may introduce a systematic bias towards conservative estimations. Pronounced diurnal variability is common in shallow, eutrophic lakes, where nocturnal respiration often drives CO_2 fluxes significantly higher than daytime values (Podgrajsek et al., 2015; Zhang et al., 2019; Wang et al., 2024; Zhao et al., 2024). Recent quantification in Lake Taihu, a comparable large shallow eutrophic lake, indicates that nocturnal fluxes are approximately 14 % higher than daytime levels (Zhao et al., 2024). Applying this specific error margin to our study suggests that our reported values likely represent a conservative lower bound, potentially underestimating the net carbon source strength by 7 %. To resolve this, future protocols should incorporate high-frequency (e.g., hourly) automated monitoring to capture the full diel metabolic cycles.

Third, constraints related to biological data resolution warrant consideration, which inevitably influenced our modeling capabilities. We utilized widely accepted NDVI and VGPM-derived GPP as robust proxies to infer the "autotrophic sink collapse" and the Stage III rebound. However, even these well-established remote sensing metrics cannot fully substitute for high-frequency in situ measurements of macrophyte biomass and community structure. This data gap likely explains the performance disparity observed in our RF analysis. While the model demonstrated high predictive accuracy for the nutrient-driven LYC, its performance was comparatively lower for the DTH dataset. This disparity is likely attributable to the semi-enclosed, macrophyte-dominated nature of DTH, where micro-scale heterogeneity and restricted hydrodynamics remain uncaptured by aggregate remote sensing predictors (Luo et al., 2020; Pu et al., 2022). Consequently, the omission of these fine-scale biotic and hydrologic variables limits our ability to fully resolve the model residuals in DTH. Future research should prioritize integrating process-based ecosystem modeling with high-resolution monitoring to explicitly quantify these phase-specific biological controls.

5. Conclusion

This 16-year study (2000–2015) elucidates the divergent CO_2 dynamics in two typical aquaculture-affected lakes, identifying both distinct spatial patterns and complex temporal trajectories. Both LYC and DTH were confirmed as net CO_2 sources, yet they exhibited a threefold disparity in emission magnitude (108 ± 56 g C m^{-2} yr^{-1} in LYC vs 37 ± 24 g C m^{-2} yr^{-1} in DTH). This spatial heterogeneity was primarily driven by the higher anthropogenic nutrient loading in LYC, compounded by synergistic effects of aquaculture residues and external catchment inputs.

Crucially, long-term monitoring in LYC revealed a counter-intuitive "V-shaped" emission trajectory following the phased pen retreat. While emissions initially declined by 54 % during the active removal phase, a distinct 56 % rebound occurred in the post-restoration phase. This pattern highlights a critical mechanism: the "autotrophic sink collapse" can override the benefits of nutrient reduction, shifting the ecosystem toward a respiration-dominated state. This finding serves as a cautionary tale that "pollutant removal" alone does not guarantee carbon mitigation.

Furthermore, our RF analysis challenges the conventional application of aquaculture area, demonstrating that area acts not merely as a static scalar for total load calculations but as a dynamic driver of emission intensity itself. Consequently, future carbon accounting frameworks must integrate the non-linear coupling of area and intensity to improve accuracy. Ultimately, our findings highlight that the re-establishment of aquatic vegetation, rather than nutrient reduction alone, is the critical ecological prerequisite for preventing emission rebounds and recovering the ecosystem's long-term carbon sequestration capacity.

CRediT authorship contribution statement

Jiayu Zhao: Writing – original draft, Funding acquisition, Formal analysis, Data curation, Conceptualization. **Mi Zhang:** Writing – review & editing, Methodology, Formal analysis. **Wei Xiao:** Writing – review & editing, Project administration, Funding acquisition. **Pei Ge:** Investigation. **Juhua Luo:** Data curation. **Minliang Jiang:** Data curation. **Cheng Hu:** Writing – review & editing, Data curation. **Delin Li:** Funding acquisition, Data curation. **Tianyu Zhang:** Funding acquisition. **Hongtao Duan:** Data curation. **Qitao Xiao:** Writing – review & editing, Methodology, Funding acquisition, Data curation, Conceptualization. **Xuhui Lee:** Writing – review & editing, Formal analysis, Data curation.

Declaration of competing interest

The authors declare that they have no known competing financial interests or personal relationships that could have appeared to influence the work reported in this paper.

Acknowledgements

This research was supported jointly by the National Natural Science Foundation of China (42425104, 42401111, 42271114, 42205025 and 42271377), the "333 Project" of Jiangsu Province (BRA2022023), the National Foreign Experts Program (No. S20240134), Key Laboratory of Ecosystem Carbon Source and Sink, China Meteorological Administration (ECSS-CMA202302, ECSS-CMA202404), the Youth Innovation Promotion Association of CAS (2023329), and the Program for scientific research startup funds of Guangdong Ocean University (060302032302).

Supplementary materials

Supplementary material associated with this article can be found, in the online version, at doi:10.1016/j.watres.2026.125562.

Data availability

Data will be made available on request.

References

Abril, G., Bouillon, S., Darchambeau, F., Teodoru, C.R., Marwick, T.R., Tamooh, F., Omengo, F.O., Geeraert, N., Deirmendjian, L., Polsenaere, P., Borges, A.V., 2015. Technical note: large overestimation of pCO_2 calculated from pH and alkalinity in acidic, organic-rich freshwaters. Biogeosciences 12, 67–78. https://doi.org/10.5194/bg-12-67-2015.

Borges, A.V., Deirmendjian, L., Bouillon, S., Okello, W., Lambert, T., Roland, F., Razanamahandry, V.F., Voarintsoa, N.R.G., Darchambeau, F., Kimire, I., Descy, J.P., Allen, G.H., Morana, C., 2022. Greenhouse gas emissions from African lakes are no longer a blind spot. Sci. Adv. 8, 8716.

Brigham, B.A., Bird, J.A., Juhl, A.R., Zappa, C.J., Montero, A.D., O'Mullan, G.D., 2019. Anthropogenic inputs from a coastal megacity are linked to greenhouse gas concentrations in the surrounding estuary. Limnol. Oceanogr. 64, 2497–2511.

Chen, G., Bai, J., Bi, C., Wang, Y., Cui, B., 2023. Global greenhouse gas emissions from aquaculture: a bibliometric analysis. Agric. Ecosyst. Environ. 348, 108405.

Chen, X., Wang, Y., Sun, T., Huang, Y., Chen, Y., Zhang, M., Ye, C., 2021. Effects of sediment dredging on nutrient release and eutrophication in the gate-controlled estuary of Northern Taihu Lake. J. Chem. 1, 7451832.

Chen, Y., Dong, S., Wang, F., Gao, Q., Tian, X., 2016. Carbon dioxide and methane fluxes from feeding and no-feeding mariculture ponds. Environ. Pollut. 212, 489–497.

China Fishery Statistical Yearbook, 2023. China Agriculture Press, Beijing.

Chmiel, H.E., Kokic, J., Denfeld, B.A., Einarsdóttir, K., Wallin, M.B., Isidorova, A., Koehler, B., Steinwall, S., Sobek, S., 2016. The role of sediments in the carbon budget of a small boreal lake. Limnol. Oceanogr. 61 (5), 1814–1825.

Cole, J.J., Caraco, N.F., 1998. Atmospheric exchange of carbon dioxide in a low-wind oligotrophic lake measured by the addition of SF_6. Limnol. Oceanogr. 43, 647–656.

Cole, J.J., Prairie, Y.T., Caraco, N.F., McDowell, W.H., Tranvik, L.J., Striegl, R.G., Duarte, C.M., Kortelainen, P., Downing, J.A., Middelburg, J.J., Melack, J., 2007. Plumbing the global carbon cycle: integrating inland waters into the terrestrial carbon budget. Ecosystems 10, 171–184.

Del Giorgio, P., Williams, P. (Eds.), 2005. Respiration in Aquatic Ecosystems. OUP Oxford.

DelSontro, T., Beaulieu, J.J., Downing, J.A., 2018. Greenhouse gas emissions from lakes and impoundments: upscaling in the face of global change. Limnol. Oceanogr. Lett. 3, 64–75.

Deng, Y., Zhang, Y., Li, D., Shi, K., Podgorski, D.C., Tang, X., Qin, B., 2017. Temporal and spatial dynamics of phytoplankton primary production in Lake Taihu derived from MODIS data. Remote Sens. 9, 195.

Dong, B., Xi, Y., Cui, Y., Peng, S., 2022. Quantifying methane emissions from aquaculture ponds in China. Environ. Sci. Technol. 57, 1576–1583.

Duan, H., Xiao, Q., Qi, T., 2023. Measuring lake carbon dioxide from space: opportunities and challenges. Innov. Geosci. 1, 100025.

Duan, T., Feng, J., Chang, X., Li, Y., 2022. Evaluation of the effectiveness and effects of long-term ecological restoration on watershed water quality dynamics in two eutrophic river catchments in Lake Chaohu Basin. China. Ecol. Indic. 145, 109592.

FAO, 2024. The State of World Fisheries and Aquaculture 2024: Blue Transformation in Action. FAO, Rome.

Finlay, K., Vogt, R.J., Bogard, M.J., Wissel, B., Tutolo, B.M., Simpson, G.L., Leavitt, P.R., 2015. Decrease in CO_2 efflux from northern hardwater lakes with increasing atmospheric warming. Nature 519, 215–218.

Gao, Y., Jia, J., Lu, Y., Yang, T., Lyu, S., Shi, K., Zhou, F., Yu, G., 2021. Determining dominating control mechanisms of inland water carbon cycling processes and associated gross primary productivity on regional and global scales. Earth-Sci. Rev. 213, 103497.

Golub, M., Desai, A.R., McKinley, G.A., Remucal, C.K., Stanley, E.H., 2017. Large uncertainty in estimating pCO_2 from carbonate equilibria in lakes. J. Geophys. Res. Biogeosci. 122, 2909–2924.

Grasset, C., Mesman, J.P., Tranvik, L.J., Maranger, R., Sobek, S., 2025. Contribution of lake littoral zones to the continental carbon budget. Nat. Geosci. 18, 1–6.

Gudasz, C., Bastviken, D., Steger, K., Premke, K., Sobek, S., Tranvik, L.J., 2010. Temperature-controlled organic carbon mineralization in lake sediments. Nature 466 (7305), 478–481.

Hall, B.D., Hesslein, R.H., Emmerton, C.A., Higgins, S.N., Ramlal, P., Paterson, M.J., 2019. Multidecadal carbon sequestration in a headwater boreal lake. Limnol. Oceanogr. 64, S150–S165.

Hao, Z., Chen, S., Zhang, Q., Liu, B., Chen, S., 2025. Enhanced carbon sequestration potential following sediment dredging in river ecosystems: insights into CO_2 fluxes, phytoplankton, and carbon fixation pathway responses. Environ. Sci. Technol. 59, 14075–14088. https://doi.org/10.1021/acs.est.5c05177.
Holgerson, M.A., Raymond, P.A., 2016. Large contribution to inland water CO_2 and CH_4 emissions from very small ponds. Nat. Geosci. 9, 222–226.
Hong, L., Hu, C., Jiang, M., Shi, X., Luo, J., Xiao, Q., 2025. Long-term carbon dioxide dynamics variability at submerged macrophyte habitat of a subtropical shallow lake. J. Hydrol. 632, 133950.
Jeppesen, E., Søndergaard, M., Meerhoff, M., Lauridsen, T.L., Jensen, J.P., 2007. Shallow lake restoration by nutrient loading reduction—Some recent findings and challenges ahead. Hydrobiologia 584 (1), 239–252.
Jia, J., Dungait, J.A., Lu, Y., Cui, T., Yu, G., Gao, Y., 2023. Inland water metabolic carbon processes and associated biological mechanisms that drive carbon source-sink instability. Innov. Geosci. 1 (3), 100035-1.
Jia, J., Gao, Y., Zhou, F., Shi, K., Qin, B., Zhang, Y., Zhu, G., 2020. Identifying the main drivers of change of phytoplankton community structure and gross primary productivity in a river-lake system. J. Hydrol. 583, 124633.
Jongejans, L.L., Liebner, S., Knoblauch, C., Mangelsdorf, K., Ulrich, M., Grosse, G., Strauss, J., 2021. Greenhouse gas production and lipid biomarker distribution in Yedoma and Alas thermokarst lake sediments in Eastern Siberia. Glob. Change Biol. 27 (12), 2822–2839.
Kankaala, P., Huotari, J., Tulonen, T., Ojala, A., 2013. Lake-size dependent physical forcing drives carbon dioxide and methane effluxes from lakes in a boreal landscape. Limnol. Oceanogr. 58, 1915–1930.
Kim, Y., Johnson, M.S., Knox, S.H., Black, T.A., Dalmagro, H.J., Kang, M., Baldocchi, D., 2020. Gap-filling approaches for eddy covariance methane fluxes: a comparison of three machine learning algorithms and a traditional method with principal component analysis. Glob. Change Biol. 26, 1499–1518.
Kosten, S., Roland, F., Da Motta Marques, D.M.L., Van Nes, E.H., Mazzeo, N., Sternberg, L.S.L., Scheffer, M., Cole, J.J., 2010. Climate-dependent CO_2 emissions from lakes. Glob. Biogeochem. Cycles 24. GB2007.
Kosten, S., Almeida, R.M., Barbosa, I., Mendonca, R., Santos Muzitano, I., Sobreira Oliveira-Junior, E., Vroom, R.J.E., Wang, H.J., Barros, N., 2020. Better assessments of greenhouse gas emissions from global fish ponds needed to adequately evaluate aquaculture footprint. Sci. Total Environ. 748, 141247.
Lauerwald, R., Allen, G.H., Deemer, B.R., Liu, S., Maavara, T., Raymond, P., Alcott, L., Bastviken, D., Hastie, A., Holgerson, M.A., 2023. Inland water greenhouse gas budgets for RECCAP2: 1. State-of-the-art of global scale assessments. Glob. Biogeochem. Cycles 37, e2022GB007657.
Li, S., Bush, R.T., Santos, I.R., Zhang, Q., Song, K., Mao, R., Wen, Z., Lu, X., 2018. Large greenhouse gases emissions from China's lakes and reservoirs. Water Res. 147, 13–24.
Li, Y., Gu, X., Zeng, Q., Jia, B., Zi, X., Chen, H., Mao, Z., Ge, Y., 2023. Fluctuations of nutrient concentrations and their influencing factors under various net-pen aquaculture scales in East Lake Taihu from 1990 to 2021. J. Lake Sci. 35, 155–167. Chinese.
Lin, Q., Zhang, K., McGowan, S., Capo, E., Shen, J., 2021. Synergistic impacts of nutrient enrichment and climate change on long-term water quality and ecological dynamics in contrasting shallow-lake zones. Limnol. Oceanogr. 66 (9), 3271–3286.
Liu, C., Xu, J., Xu, K., Yu, J., 2024a. Mapping large-scale aquaculture ponds in Jiangsu Province, China: an automatic extraction framework based on Sentinel-1 time-series imagery. Aquaculture 581, 740441.
Liu, H., Fu, C., Ding, G., Fang, Y., Yun, Y., Norra, S., 2019. Effects of hairy crab breeding on drinking water quality in a shallow lake. Sci. Total Environ. 662, 48–56.
Liu, J., Neogi, S., Lai, D.Y., 2025a. Ecosystem-scale carbon dioxide, methane and water vapor fluxes from subtropical brackish fishponds: temporal variability, environmental drivers, and implications for nature-based climate solutions. Earth's Future 13, e2024EF005277.
Liu, L., Yang, K., Li, L., Liu, W., Yuan, H., Han, Y., Xu, C., Li, S., Zhang, W., Jia, Y., 2024b. The aeration and dredging stimulate the reduction of pollution and carbon emissions in a sediment microcosm study. Sci. Rep. 14 (1), 26172.
Liu, S., Wang, J., Xu, W., Zhang, P., Zhang, S., Chen, X., Zhang, Z., Huang, W., Zheng, W., Xia, X.H., 2025b. Human activities reshape greenhouse gas emissions from inland waters. Glob. Change Biol. 31, e17239.
Luo, J., Li, X., Ma, R., Li, F., Duan, H., Hu, W., Qin, B., Huang, W., 2016. Applying remote sensing techniques to monitoring seasonal and interannual changes of aquatic vegetation in Taihu Lake. China. Ecol. Indic. 60, 503–513.
Luo, J., Pu, R., Ma, R., Wang, X., Lai, X., Mao, Z., Zhang, L., Peng, Z.L., Sun, Z., 2020. Mapping long-term spatiotemporal dynamics of pen aquaculture in a shallow lake: less aquaculture coming along better water quality. Remote Sens. 12, 1866.
Maberly, S.C., Barker, P.A., Stott, A.W., De Ville, M.M., 2013. Catchment productivity controls CO_2 emissions from lakes. Nat. Clim. Change. 3, 391–394.
Martinsen, K.T., Kragh, T., Sand-Jensen, K., 2020. Carbon dioxide partial pressure and emission throughout the Scandinavian stream network. Glob. Biogeochem. Cycles 34 e2020GB006703.
Natchimuthu, S., Panneer Selvam, B., Bastviken, D., 2014. Influence of weather variables on methane and carbon dioxide flux from a shallow pond. Biogeochemistry 119 (1), 403–413.
Nijman, T.P., Lemmens, M., Lurling, M., Kosten, S., Welte, C., Veraart, A.J., 2022. Phosphorus control and dredging decrease methane emissions from shallow lakes. Sci. Total Environ. 847, 157584.
Pi, X., Luo, Q., Feng, L., Xu, Y., Tang, J., Liang, X., Ma, E., Cheng, R., Fensholt, R., Brandt, M., Cai, X., Gibson, L., Liu, J., Zheng, C., Li, W., Bryan, B., 2022. Mapping global lake dynamics reveals the emerging roles of small lakes. Nat. Commun. 13, 5777.
Podgrajsek, E., Sahlée, E., Rutgersson, A., 2015. Diel cycle of lake-air CO_2 flux from a shallow lake and the impact of waterside convection on the transfer velocity. J. Geophys. Res. Biogeosci. 120, 29–38.
Poikane, S., Kelly, M.G., Free, G., Carvalho, L., Hamilton, D.P., Katsanou, K., Hilt, S., Kolada, A., Willby, N., Vicente, E., Guan, X., Irvine, K., 2024. A global assessment of lake restoration in practice: new insights and future perspectives. Ecol. Indic. 158, 111330.
Pu, Y., Zhang, M., Jia, L., Zhang, Z., Xiao, W., Liu, S., Zhao, J., Xie, Y., Lee, X., 2022. Methane emission of a lake aquaculture farm and its response to ecological restoration. Agric. Ecosyst. Environ. 330, 107883.
Raymond, P.A., Hartmann, J., Lauerwald, R., Sobek, S., McDonald, C., Hoover, M., Butman, D., Striegl, R., Mayorga, E., Humborg, C., Kortelainen, P., Durr, H., Meybeck, M., Ciais, P., Guth, P., 2013. Global carbon dioxide emissions from inland waters. Nature 503, 355–359.
Shi, X., Sun, J., Wang, J., Lucas-Borja, M.E., Pandey, A., Wang, T., Huang, Z., 2023. Tree species richness and functional composition drive soil nitrification through ammonia-oxidizing archaea in subtropical forests. Soil Biol. Biochem. 187, 109211.
Song, C., Liu, S., Wang, G., Zhang, L., Rosentreter, J.A., Zhao, G., Yang, Q., Lai, D.Y.F., Raymond, P.A., Karlsson, J., 2024. Inland water greenhouse gas emissions offset the terrestrial carbon sink in the northern cryosphere. Sci. Adv. 10, eadp0024.
Tong, Y.J., Lin, C., Song, K., Jiang, T.C., Ma, R.H., Cui, W.Z., Ma, D.H., Chen, J.C., Wang, Z.X., Bai, X.F., 2025. Reconstructing coastal ponds functional classification: integration of multi-feature remote sensing. Ecol. Inform. 91, 103370.
Waldemer, C., Koschorreck, M., 2023. Spatial and temporal variability of greenhouse gas ebullition from temperate freshwater fish ponds. Aquaculture 574, 739656.
Wang, Y., Ma, B., Xu, Y.J., Shen, S., Huang, X., Wang, Y., Ye, S., Tian, X., Zhang, Y., Wang, T., Li, S., 2024. Eutrophication and dissolved organic matter exacerbate the diel discrepancy of CO_2 emissions in China's largest urban lake. Environ. Sci. Technol. 58, 20968–20978.
Xiao, Q., Zhang, M., Hu, Z., Gao, Y., Hu, C., Liu, C., Liu, S., Zhang, Z., Zhao, J., Xiao, W., Lee, X., 2017. Spatial variations of methane emission in a large shallow eutrophic lake in subtropical climate. J. Geophys. Res. Biogeosci. 122, 1597–1614.
Xiao, Q., Duan, H., Qi, T., Hu, Z., Liu, S., Zhang, M., Lee, X., 2020. Environmental investments decreased partial pressure of CO_2 in a small eutrophic urban lake: evidence from long-term measurements. Environ. Pollut. 263, 114433.
Xiao, Q., Xiao, W., Luo, J., Qiu, Y., Hu, C., Zhang, M., Qi, T., Duan, H., 2023. Management actions mitigate the risk of carbon dioxide emissions from urban lakes. J. Environ. Manage 344, 118626.
Xiao, Q., Xu, X., Qi, T., Luo, J., Lee, X., Duan, H., 2024a. Lakes shifted from a carbon dioxide source to a sink over past two decades in China. Sci. Bull. 69, 1857–1861.
Xiao, Q., Zhou, Y., Luo, J., Hu, C., Duan, H., Qiu, Y., Zhang, M., Hu, Z., Xiao, W., 2024b. Low carbon dioxide emissions from aquaculture farm of lake revealed by long-term measurements. Agric. Ecosyst. Environ. 363, 108851.
Xiao, W., Liu, S.D., Li, H.C., Xiao, Q.T., Wang, W., Hu, Z.H., Hu, C., Gao, Y.Q., Shen, J., Zhao, X.Y., Zhang, M., Lee, X.H., 2014. A flux-gradient system for simultaneous measurement of the CH_4, CO_2, and H_2O fluxes at a lake-air interface. Environ. Sci. Technol. 48, 14490–14498.
Yang, P., Zhang, Y., Lai, D.Y.F., Tan, L., Jin, B., Tong, C., 2018. Fluxes of carbon dioxide and methane across the water-atmosphere interface of aquaculture shrimp ponds in two subtropical estuaries: the effect of temperature, substrate, salinity and nitrate. Sci. Total Environ. 635, 1025–1035.
Yang, P., Zhang, L., Lin, Y., Yang, H., Lai, D.Y., Tong, C., Zhang, Y., Tan, L., Zhao, G., Tang, K.W., 2024. Significant inter-annual fluctuation in CO_2 and CH_4 diffusive fluxes from subtropical aquaculture ponds: implications for climate change and carbon emission evaluations. Water Res. 249, 120943.
Yin, Y., Gao, M., Cao, X., Wei, J., Zhong, X., Li, S., Peng, K., Gao, J., Gong, Z., Cai, Y., 2024. Restore polder and aquaculture enclosure to the lake: balancing environmental protection and economic growth for sustainable development. Sci. Total Environ. 933, 173036.
Yuan, J., Xiang, J., Liu, D.Y., Kang, H., He, T., Kim, S., Lin, Y., Freeman, C., Ding, W., 2019. Rapid growth in greenhouse gas emissions from the adoption of industrial-scale aquaculture. Nat. Clim. Change. 9, 318–322.
Yuan, J., Dong, Y., Li, J., Liu, D., Xiang, J., He, T., Kang, H., Ding, W., 2025. Foregone carbon sequestration dominates greenhouse gas footprint in aquaculture associated with coastal wetland conversion. Nat. Food. 6, 587–596.
Yvon-Durocher, G., Caffrey, J.M., Cescatti, A., Dossena, M., del Giorgio, P., Gasol, J.M., Montoya, J.M., Pumpanen, J., Staehr, P.A., Trimmer, M., Woodward, G., Allen, A.P., 2012. Reconciling the temperature dependence of respiration across timescales and ecosystem types. Nature 487 (7408), 472–476.
Yvon-Durocher, G., Hulatt, C.J., Woodward, G., Trimmer, M., 2017. Long-term warming amplifies shifts in the carbon cycle of experimental ponds. Nat. Clim. Chang. 7 (3), 209–213.
Zhao, F., Huang, Z., Wang, Q., Wang, X., Wang, Y., Zhang, Q., He, W., Tong, Y., 2024. Seasonal pattern of diel variability of CO_2 efflux from a large eutrophic lake. J. Hydrol. 645, 132259. https://doi.org/10.1016/j.jhydrol.2024.132259.
Zhao, J., Zhang, M., Pu, Y., Jia, L., Xiao, W., Zhang, Z., Lee, X., 2025. Dynamic and high methane emission flux in pond and lake aquaculture. J. Hydrol. 643, 132765.
Zhang, M., Xiao, Q., Zhang, Z., Gao, Y., Zhao, J., Pu, Y., Wang, W., Xiao, W., Liu, S., Lee, X., 2019. Methane flux dynamics in a submerged aquatic vegetation zone in a subtropical lake. Sci. Total Environ. 672, 400–409. https://doi.org/10.1016/j.scitotenv.2019.03.466.
Zhang, Y., Qin, Z., Li, T., Zhu, X., 2022a. Carbon dioxide uptake overrides methane emission at the air-water interface of algae-shellfish mariculture ponds: evidence from eddy covariance observations. Sci. Total Environ. 815, 152867.
Zhang, Y., Tang, K.W., Yang, P., Yang, H., Tong, C., Song, C., Tan, L., Zhao, G., Zhou, X., Sun, D., 2022b. Assessing carbon greenhouse gas emissions from aquaculture in

China based on aquaculture system types, species, environmental conditions and management practices. Agric. Ecosyst. Environ. 338, 108110.

Zhang, Y., Li, S., Yang, P., Zhang, Y., Lu, X., Tang, K.W., Yang, H., Wang, Z., Yu, G., Tong, C., Zhang, Z., Jiang, P., Wang, Y., Zhao, J., Yang, X., Zhang, L., Xia, X., 2026a. Revealing the unrecognized climate burden of aquaculture systems: a global insight into greenhouse gas emissions and mitigation strategies. Water Res 292, 125389. https://doi.org/10.1016/j.watres.2026.125389.

Zhang, Z., Xia, X., Liu, S., Wang, J., Xu, W., McDowell, W.H., Tian, H., Yang, Z., 2026b. Human-impacted lakes contribute over one-third of global lake greenhouse gas emissions. One Earth 9, 101568. https://doi.org/10.1016/j.oneear.2025.101568.